Int. J. Heat Mass Transfer. Vol. 33, No. 5, pp. 901–915, 1990
Printed in Great Britain

0017–9310/90 $3.00 + 0.00

Superposition technique for radiative equilibrium in rectangular enclosures with complex boundary conditions

W. W. YUEN and E. E. TAKARA
Department of Mechanical and Environmental Engineering, University of California at Santa Barbara, Santa Barbara, CA 93106, U.S.A.

(*Received* 26 *April* 1989 *and in final form* 10 *August* 1989)

Abstract—Superposition of fundamental solutions is used to find temperature and heat flux distributions in gray walled two-dimensional rectangular enclosures with a gray absorbing–emitting, isotropically scattering medium. The fundamental solutions are temperature and heat flux distributions for enclosures with black boundaries and a step change in temperature over a finite wall interval. They are found using a variation of the conventional zonal method. Detailed heat flux and temperature distributions for basic cases are presented to illustrate the simplicity of the superposition procedure. Based on these results, the effects of surface boundary conditions on the temperature distribution and heat transfer are discussed.

1. INTRODUCTION

THE IMPORTANCE of radiative heat transfer in many engineering systems is well known. Until recently, quantitative illustration of these effects has been difficult because of the mathematical complexity of radiative heat transfer. In many practical problems it is necessary to analyze radiative heat transfer in a multi-dimensional enclosure with reflecting and emitting boundaries. The temperature might be specified on some surfaces, while on others the heat transfer rate or a heat transfer coefficient might be given. The problem of radiative equilibrium in a two-dimensional rectangular enclosure has been solved many times [1–9]. One widely used analysis technique is the zonal method described in ref. [10] and its variations, as in refs. [4, 6, 7]. The other widely used family of techniques is the differential methods [1–3]. Regardless of the method used there is a facet of this problem which has been largely neglected: in the absence of conduction and convection, radiation is a linear process. Therefore, the method of superposition can be used to find solutions to problems with complex boundary conditions.

Previous works [1–9] solved for the temperature and heat flux distributions for basic enclosures with one 'hot' wall, a wall at unit temperature, and three cold walls, walls with zero temperature. The temperature and heat flux distributions for more complex enclosures with more than one 'hot' wall are found by superimposing the distributions of the basic enclosures. This is inefficient because nearly identical distributions must be generated if the wall emissivities change or boundary conditions become complicated. Modest [11] and Crosbie and Koewing [12] used a more sophisticated superposition technique, similar to the one presented in this work, to analyze two-dimensional plane layers. The total exchange area method described by Hottel and Sarofim [10] and its variants [13, 14] is another advanced superposition technique; however, it has the computational inefficiency of refs. [1–9]. The advantage of the total exchange method is that it is valid even in multi-mode heat transfer. Direct superposition is not valid in these non-linear situations so either the total exchange method or others as in refs. [15–18] must be used for solution.

In multi-dimensional enclosures with reflecting boundaries and/or heat flux boundary conditions surface radiosity, not surface temperature or heat flux, is the 'natural' boundary condition. The radiosities, not the temperature or heat flux, must be superimposed. Although the previous works [1–9] implicitly superimpose the radiosities, they do not take advantage of the possibility that the radiosities themselves can be obtained through superposition. This is a major limitation; in this work a superposition procedure based on surface radiosity is developed. The radiosity at a diffusely reflecting surface is a function of both its temperature and heat flux. Since one of these is unknown, a system of integral equations has to be solved to generate the heat flux and temperature distributions.

The remainder of this paper is organized in three sections. First, the superposition procedure will be illustrated mathematically. For a rectangular enclosure, the fundamental solutions which are required for this superposition procedure will be identified. Second, a solution method which is extremely efficient in generating these fundamental solutions will be described. The method is a generalization of a technique which has been shown to be effective [7, 8, 17] for two-dimensional radiative heat transfer with black isothermal boundaries. Finally, solutions for selected

NOMENCLATURE

$A_{i,j,m,n}$ coefficient defined by equation (18) and derived in the Appendix
$B_{i,j}$ coefficient defined by equations (18) and (A23)
$f(L_1, L_2, \lambda, y, z)$, $f'(L_1, L_2, \lambda, y, z)$ functions defined by equation (4a)
$F(\lambda_{y,i}, y, z)$, $F'(\lambda_{z,j}, y, z)$ functions defined by equations (7a) and (7b)
$F_{m,n}$ $F(\lambda_i, \eta_m, \zeta_n)$
$\mathbf{g}(\lambda_{y,i}, y, z)$, $\mathbf{g}'(\lambda_{z,j}, y, z)$ heat flux vectors the components g_y, g_z, g'_y, g'_z of which are defined in equations (4b) and (4c)
$\mathbf{G}(\lambda_{y,i}, y, z)$, $\mathbf{G}'(\lambda_{z,j}, y, z)$ functions defined by equations (8a) and (8b)
$G_{i,j,k}(x, y)$ function defined by equation (A11)
H_{ij} parameters defined by equations (A2)–(A5)
$J(y, z)$ surface radiosity
K_t extinction coefficient
L_1 optical thickness in the y-direction, K_tY
L_2 optical thickness in the z-direction, K_tZ
$M_{ij}(x, y)$ function defined by equation (A13)
$N_{m,n}$ function defined by equation (A1)
$P^{i,j}_{m,n}$ parameters defined by equations (A15)–(A18)
$\mathbf{q}(y, z)$ heat flux vector
q_n heat flux in direction normal to wall
r radial coordinate used in equations (11), (15) and (16) and Fig. 2
$S_n(ax)$ exponential integral function, $(2x^n/\pi)\int_0^\infty (\exp(-a\sqrt{(\tau^2+x^2)})/(\tau^2+x^2)^{1.2(n+1)})\,d\tau$, $a, \tau \geqslant 0$; $n = 0, 1, \ldots$
y coordinate
Y dimension of enclosure in the y-direction
z coordinate
Z dimension of enclosure in the z-direction.

Greek symbols

β_i angles defined by equations (A7)–(A10)
ε emissivity
λ integration variable used in equations (4a)–(4c) and (5a)–(5c)
η non-dimensional coordinate in the y-direction, y/Y
ζ non-dimensional coordinate in the z-direction, z/Z
θ emissive power
θ_w emissive power of wall
ϕ angular coordinate used in equations (11), (15) and (16) and Fig. 2
ϕ_1 angle defined by equation (13)
ϕ_2 angle defined by equation (14).

enclosures will be presented to illustrate the effectiveness of the present solution technique.

While the present approach can be readily applied to an enclosure with arbitrary surface emissive power and emissivity (or heat flux) distribution, only three specific cases are presented to illustrate the general effect of surface emissivity and heat flux boundary conditions on multi-dimensional radiative heat transfer. In the first analysis, the walls are assumed to be diffusely reflecting and emitting with the bottom wall an isothermal surface with unit emissive power, other walls cold. In the second case, the bottom wall is assumed to be black, nonisothermal with constant unit heat flux and the other walls black and cold. Lastly, the case of an isothermal bottom wall in combination with two cold walls and one adiabatic diffusely reflecting or specularly reflecting side wall is considered. These cases are selected because solutions to the first analysis have been reported by other investigators [2–4, 6]. The efficiency and accuracy of the present approach can be seen in direct comparison. The second analysis demonstrates the ease of applying the present technique to enclosures with heat flux boundary conditions. Though less common than temperature boundary conditions, there is literature in this area from Gebhart [19] in 1961, for enclosures with non-participating media, to Sokmen and Razzaque [18] in 1987, for combined conduction and radiation heat transfer. The last analysis reemphasizes the importance of boundary conditions, the difference between specular and diffuse reflection in multi-dimensional radiative heat transfer.

2. SUPERPOSITION PROCEDURE

Consider a rectangular enclosure with a coordinate system as shown in Fig. 1. All boundaries are assumed to be diffusely emitting and reflecting surfaces. From standard references [10, 20], it can be readily shown that the radiosity at the boundary is given by

$$J(s) = \theta_w(s) - \frac{1-\varepsilon(s)}{\varepsilon(s)} q_n(s) \qquad (1)$$

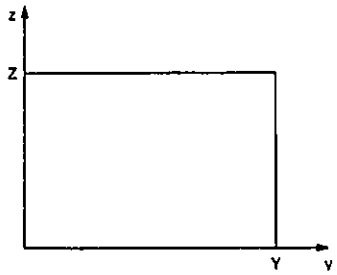

FIG. 1. Geometry and coordinate system for the two-dimensional enclosure.

where s is a coordinate measured along the boundary, $\theta_w(s)$, $\varepsilon(s)$ are the emissive power and emissivity of the boundary at s and $q_n(s)$ is the radiative heat flux in the direction normal to the boundary. Using equation (1) the boundary radiosity $J(s)$ for an enclosure with temperature boundary conditions can be found using superposition. This can be seen as follows.

(1) For an assumed boundary radiosity distribution, $J(s)$, the temperature and heat flux distributions in the medium can be found. Therefore, equations for the temperature and heat flux distributions can be derived in terms of an unknown radiosity distribution $J(s)$.

(2) The expressions for surface heat flux $q_n(s)$ and the given boundary condition $\theta_w(s)$ can be substituted into equation (1). The result is a set of equations for the unknown radiosity distribution $J(s)$.

For heat flux boundary conditions the same reasoning applies. The expressions for surface heat flux $q_n(s)$ are equated to the given boundary condition $q_n(s)$.

2.1. *Case* 1: *hot diffuse bottom wall and three cold diffuse walls*

In this case, the bottom wall is assumed to be gray and hot with $\theta(y, 0) = 1.0$ and emissivity ε_0 and the other three walls cold with $\theta(y, Z) = \theta(0, z) = \theta(Y, z) = 0$ and emissivity ε_1. Equation (1) becomes

$$J(y,0) = 1.0 - \frac{1-\varepsilon_0}{\varepsilon_0} q_z(y,0) \tag{2a}$$

$$J(y,Z) = \frac{1-\varepsilon_1}{\varepsilon_1} q_z(y,Z) \tag{2b}$$

$$J(0,z) = -\frac{1-\varepsilon_1}{\varepsilon_1} q_y(0,z) \tag{2c}$$

and

$$J(0,z) = J(Y,z). \tag{2d}$$

To generate a set of integral equations for the unknown radiosity distribution, two sets of fundamental solutions are introduced. Specifically, $f(L_1, L_2, \lambda, y, z)$ and $g(L_1, L_2, \lambda, y, z)$ are the emissive power and heat flux distributions for a rectangular enclosure with a gray medium and black walls. The bottom wall ($z = 0$) is 'hot' with unit emissive power from $y = 0$ to λ; the remainder of the bottom wall and the other three walls are 'cold' with zero emissive power. These fundamental solutions are used to account for the 'non-zero' boundary conditions of the top and bottom walls ($z = 0$ and Z). To account for the 'non-zero' boundary conditions at the two side walls ($y = 0$ and Y), the functions $f^1(L_1, L_2, \lambda, y, z)$ and $g^1(L_1, L_2, \lambda, y, z)$ are introduced. They are the emissive power and heat flux distribution for an enclosure which has a 'hot' side wall ($y = 0$) with unit emissive power from $z = 0$ to λ the remainder of the wall and the other three walls 'cold' with zero emissive power. The two sets of fundamental solutions are related as follows:

$$f^1(L_1, L_2, \lambda, y, z) = f(L_2, L_1, \lambda, z, y) \tag{3a}$$

$$g_y^1(L_1, L_2, \lambda, y, z) = g_z(L_2, L_1, \lambda, z, y) \tag{3b}$$

$$g_z^1(L_1, L_2, \lambda, y, z) = g_y(L_2, L_1, \lambda, z, y). \tag{3c}$$

The emissive power $\theta(y, z)$ and heat flux $\mathbf{q}(y, z)$ for a problem with arbitrary radiosity $J(y, z)$ at the walls can be readily generated from these solutions by superposition. The specific relations are

$$\begin{aligned}\theta(y,z) = &\int_0^Y \frac{\partial}{\partial\lambda}[f(L_1, L_2, \lambda, y, z)]J(\lambda, 0)\,d\lambda \\ &+ \int_0^Y \frac{\partial}{\partial\lambda}[f(L_1, L_2, \lambda, y, Z-z)]J(\lambda, Z)\,d\lambda \\ &+ \int_0^Z \frac{\partial}{\partial\lambda}[f^1(L_1, L_2, \lambda, y, z)]J(0, \lambda)\,d\lambda \\ &+ \int_0^Z \frac{\partial}{\partial\lambda}[f^1(L_1, L_2, \lambda, Y-y, z)]J(Y, \lambda)\,d\lambda\end{aligned} \tag{4a}$$

$$\begin{aligned}q_z(y,z) = &\int_0^Y \frac{\partial}{\partial\lambda}[g_z(L_1, L_2, \lambda, y, z)]J(\lambda, 0)\,d\lambda \\ &- \int_0^Y \frac{\partial}{\partial\lambda}[g_z(L_1, L_2, \lambda, y, Z-z)]J(\lambda, Z)\,d\lambda \\ &+ \int_0^Z \frac{\partial}{\partial\lambda}[g_z^1(L_1, L_2, \lambda, y, z)]J(0, \lambda)\,d\lambda \\ &+ \int_0^Z \frac{\partial}{\partial\lambda}[g_z^1(L_1, L_2, \lambda, Y-y, z)]J(Y, \lambda)\,d\lambda\end{aligned} \tag{4b}$$

$$\begin{aligned}q_y(y,z) = &\int_0^Y \frac{\partial}{\partial\lambda}[g_y(L_1, L_2, \lambda, y, z)]J(\lambda, 0)\,d\lambda \\ &+ \int_0^Y \frac{\partial}{\partial\lambda}[g_y(L_1, L_2, \lambda, y, Z-z)]J(\lambda, Z)\,d\lambda \\ &+ \int_0^Z \frac{\partial}{\partial\lambda}[g_y^1(L_1, L_2, \lambda, y, z)]J(0, \lambda)\,d\lambda \\ &- \int_0^Z \frac{\partial}{\partial\lambda}[g_y^1(L_1, L_2, \lambda, Y-y, z)]J(Y, \lambda)\,d\lambda.\end{aligned} \tag{4c}$$

Substituting equations (4b) and (4c) into equations (2a)–(2c), one obtains

$$\begin{aligned}J(y,0) = 1 - \frac{1-\varepsilon_0}{\varepsilon_0}\Bigg\{&\int_0^Y \frac{\partial}{\partial\lambda}[g_z(L_1, L_2, \lambda, y, 0)]J(\lambda, 0)\,d\lambda \\ &- \int_0^Y \frac{\partial}{\partial\lambda}[g_z(L_1, L_2, \lambda, y, Z)]J(\lambda, Z)\,d\lambda \\ &+ \int_0^Z \Bigg(\frac{\partial}{\partial\lambda}[g_z^1(L_1, L_2, \lambda, y, 0)] \\ &+ \frac{\partial}{\partial\lambda}[g_z^1(L_1, L_2, \lambda, Y-y, 0)]\Bigg)J(0, \lambda)\,d\lambda\Bigg\}\end{aligned} \tag{5a}$$

$$J(y,Z)=\frac{1-\varepsilon_1}{\varepsilon_1}\left\{\int_0^Y\frac{\partial}{\partial\lambda}[g_z(L_1,L_2,\lambda,y,Z)]J(\lambda,0)\,d\lambda\right.$$
$$-\int_0^Y\frac{\partial}{\partial\lambda}[g_z(L_1,L_2,\lambda,y,0)]J(\lambda,Z)\,d\lambda$$
$$+\int_0^Z\left(\frac{\partial}{\partial\lambda}[g_z^1(L_1,L_2,\lambda,y,Z)]\right.$$
$$\left.\left.+\frac{\partial}{\partial\lambda}[g_z^1(L_1,L_2,\lambda,Y-y,Z)]\right)J(0,\lambda)\,d\lambda\right\}\qquad(5b)$$

$$J(0,z)=-\frac{1-\varepsilon_1}{\varepsilon_1}\left\{\int_0^Y\frac{\partial}{\partial\lambda}[g_y(L_1,L_2,\lambda,0,z)]J(\lambda,0)\,d\lambda\right.$$
$$+\int_0^Y\frac{\partial}{\partial\lambda}[g_y(L_1,L_2,\lambda,0,Z-z)]J(\lambda,Z)\,d\lambda$$
$$+\int_0^Z\left(\frac{\partial}{\partial\lambda}[g_y^1(L_1,L_2,\lambda,0,z)]\right.$$
$$\left.\left.-\frac{\partial}{\partial\lambda}[g_y^1(L_1,L_2,\lambda,Y,z)]\right)J(0,\lambda)\,d\lambda\right\}.\qquad(5c)$$

Since analytical solution to this class of problems is extremely unlikely, it is useful to express equations (5a)–(5c) as numerical quadratures. These equations become

$$J(y,0)=1$$
$$-\frac{1-\varepsilon_0}{\varepsilon_0}\left\{\sum_{i=1}^{N}G_z(L_1,L_2,\lambda_{y,i},y,0)J(\lambda_{y,i},0)\right.$$
$$-\sum_{i=1}^{N}G_z(L_1,L_2,\lambda_{y,i},y,Z)J(\lambda_{y,i},Z)$$
$$+\sum_{j=1}^{M}[G_z^1(L_1,L_2,\lambda_{z,j},y,0)$$
$$\left.+G_z^1(L_1,L_2,\lambda_{z,j},Y-y,0)]J(0,\lambda_{z,j})\right\}\qquad(6a)$$

$$J(y,Z)$$
$$=\frac{1-\varepsilon_1}{\varepsilon_1}\left\{\sum_{i=1}^{N}G_z(L_1,L_2,\lambda_{y,i},y,Z)J(\lambda_{y,i},0)\right.$$
$$-\sum_{i=1}^{N}G_z(L_1,L_2,\lambda_{y,i},y,0)J(\lambda_{y,i},Z)$$
$$+\sum_{j=1}^{M}[G_z^1(L_1,L_2,\lambda_{z,j},y,Z)$$
$$\left.+G_z^1(L_1,L_2,\lambda_{z,j},Y-y,Z)]J(0,\lambda_{z,j})\right\}\qquad(6b)$$

$$J(0,z)=$$
$$-\frac{1-\varepsilon_1}{\varepsilon_1}\left\{\sum_{i=1}^{N}G_y(L_1,L_2,\lambda_{y,i},0,z)J(\lambda_{y,i},0)\right.$$
$$+\sum_{i=1}^{N}G_y(L_1,L_2,\lambda_{y,i},0,Z-z)J(\lambda_{y,i},Z)$$
$$+\sum_{j=1}^{M}[G_y^1(L_1,L_2,\lambda_{z,j},0,z)$$
$$\left.-G_y^1(L_1,L_2,\lambda_{z,j},Y,z)]J(0,\lambda_{z,j})\right\}\qquad(6c)$$

where

$$F(\lambda_{y,i},y,z)=\frac{\partial f}{\partial\lambda}(\lambda_{y,i},y,z)\Delta\lambda_y\qquad(7a)$$

$$F^1(\lambda_{z,j},y,z)=\frac{\partial f^1}{\partial\lambda}(\lambda_{z,j},y,z)\Delta\lambda_z\qquad(7b)$$

$$\mathbf{G}(\lambda_{y,i},y,z)=\frac{\partial\mathbf{g}}{\partial\lambda}(\lambda_{y,i},y,z)\Delta\lambda_y\qquad(8a)$$

$$\mathbf{G}^1(\lambda_{z,j},y,z)=\frac{\partial\mathbf{g}^1}{\partial\lambda}(\lambda_{z,j},y,z)\Delta\lambda_z\qquad(8b)$$

with $\Delta\lambda_y=Y/N$, $\Delta\lambda_z=Z/M$, $\lambda_{y,i}=i\Delta\lambda_y$ and $\lambda_{z,j}=j\Delta\lambda_z$. Physically, $F(\lambda_{y,i},y,z)$ and $\mathbf{G}(\lambda_{y,i},y,z)$ can be interpreted as the emissive power and heat flux distribution in a black enclosure with a unit emissive power between $y=\lambda_{y,i}-\Delta\lambda_y/2$ and $y=\lambda_{y,i}+\Delta\lambda_y/2$ at the bottom wall. $F^1(\lambda_{z,j},y,z)$ and $\mathbf{G}^1(\lambda_{z,j},y,z)$ can be interpreted as the emissive power and heat flux distribution in a black enclosure with a unit emissive power between $z=\lambda_{z,j}-\Delta\lambda_z/2$ and $z=\lambda_{z,j}+\Delta\lambda_z/2$ at the side wall. Evaluating equations (6a)–(6c) at the discrete points

$$\left.\begin{matrix}(i\Delta\lambda_y,\quad 0)\\(i\Delta\lambda_y,\quad Z)\end{matrix}\right\}\quad i=0,\ldots,N$$

and

$$(0,j\Delta\lambda_z)\quad j=0,\ldots,M$$

a set of $2N+M+3$ equations are readily generated and solved for the unknown radiosity distributions. Half elements are used in the corners. The superposition is clearer when $N=M$.

2.2. *Case 2: unit heat flux at bottom wall and three cold black walls*

In a general case the discretized forms of equations (4b) and (4c) are equated to the given boundary fluxes. For a unit heat flux at the lower wall and remaining walls cold ($\theta_w=0$) and black, the governing equation is

$$1=\sum_{i=1}^{N}G_z(L_1,L_2,\lambda_{y,i},y,0)J(\lambda_{y,i},0).\qquad(9)$$

The radiosity at the three cold, black boundaries is zero. Note that $J(\lambda_{y,i},0)$ is independent of the surface emissivity ε_0. Because they are dependent only on the surface radiosity $J(\lambda_{y,i},0)$ (equations (4a)–(4c)), the temperature and heat flux distributions within the medium are also independent of surface properties. We can conclude that in an enclosure with only heat flux and cold black wall (zero radiosity) boundary conditions, the temperature and heat flux distributions are independent of the surface properties of the flux walls. This is known for the surface radiosities

of enclosures with non-participating media [10, 19, 20].

2.3. *Case 3: hot diffuse bottom wall, two cold diffuse walls and adiabatic side wall*

In this case, the boundary conditions at the top, bottom and left side wall ($y = 0$) are identical to those of case 1 while the right side wall ($y = Y$) is diffuse and adiabatic. The governing equations are

$$J(y,0) = 1 \cdot$$

$$-\frac{1-\varepsilon_0}{\varepsilon_0}\left\{\sum_{i=1}^{N} G_z(L_1,L_2,\lambda_{y,i},y,0)J(\lambda_{y,i},0) - \sum_{i=1}^{N} G_z(L_1,L_2,\lambda_{y,i},y,Z)J(\lambda_{y,i},Z) + \sum_{j=1}^{M} G_z^1(L_1,L_2,\lambda_{z,j},y,0)J(0,\lambda_{z,j}) + \sum_{j=1}^{M} G_z^1(L_1,L_2,\lambda_{z,j},Y-y,0)J(Y,\lambda_{z,j})\right\} \quad (10a)$$

$$J(y,Z) = \frac{1-\varepsilon_1}{\varepsilon_1}\left\{\sum_{i=1}^{N} G_z(L_1,L_2,\lambda_{y,i},y,Z)J(\lambda_{y,i},0) - \sum_{i=1}^{N} G_z(L_1,L_2,\lambda_{y,i},y,0)J(\lambda_{y,i},Z) + \sum_{j=1}^{M} G_z^1(L_1,L_2,\lambda_{z,j},y,Z)J(0,\lambda_{z,j}) + \sum_{j=1}^{M} G_z^1(L_1,L_2,\lambda_{z,j},Y-y,Z)J(Y,\lambda_{z,j})\right\} \quad (10b)$$

$$J(0,z) = -\frac{1-\varepsilon_1}{\varepsilon_1}\left\{\sum_{i=1}^{N} G_y(L_1,L_2,\lambda_{y,i},0,z)J(\lambda_{y,i},0) + \sum_{i=1}^{N} G_y(L_1,L_2,\lambda_{y,i},0,Z-z)J(\lambda_{y,i},Z) + \sum_{j=1}^{M} G_y^1(L_1,L_2,\lambda_{z,j},0,z)J(0,\lambda_{z,j}) - \sum_{j=1}^{M} G_y^1(L_1,L_2,\lambda_{z,j},Y,z)J(Y,\lambda_{z,j})\right\} \quad (10c)$$

$$0 = \sum_{i=1}^{N} G_y(L_1,L_2,\lambda_{y,i},Y,z)J(\lambda_{y,i},0) + \sum_{i=1}^{N} G_y(L_1,L_2,\lambda_{y,i},Y,Z-z)J(\lambda_{y,i},Z) + \sum_{j=1}^{M} G_y^1(L_1,L_2,\lambda_{z,j},Y,z)J(0,\lambda_{z,j}) - \sum_{j=1}^{M} G_y^1(L_1,L_2,\lambda_{z,j},0,z)J(Y,\lambda_{z,j}). \quad (10d)$$

Note that equation (10d) is generated from an equation with the same form as equation (10b) or (10c) with $\varepsilon = 0$; this was used in ref. [10] to model adiabatic walls.

Because of symmetry, results generated in case 1 for an enclosure with optical geometry $2L_1 \times L_2$ are equivalent to those for an enclosure with optical dimension $L_1 \times L_2$ with a perfectly reflecting specular side wall. A direct comparison with results generated by case 3 readily illustrates the difference between specular and diffuse reflection in two-dimensional radiative heat transfer.

3. FUNDAMENTAL SOLUTIONS

An enclosure with a gray, absorbing–emitting, isotropically scattering medium in radiative equilibrium is identical to an enclosure with the same optical geometry with a medium that does not scatter. This can be seen from ref. [10] where it was shown that for an isotropic medium in radiative equilibrium the volumetric radiosity is equal to the black body emissive power. An enclosure with a gray, absorbing–emitting, isotropically scattering medium can be analyzed with the zonal techniques used for a gray, absorbing–emitting medium. The method of solution developed in previous works [7, 8, 17] is now used to generate the fundamental solutions $F(\lambda_i, y, z)$ and the associated heat flux distribution $\mathbf{G}(\lambda_i, y, z)$. The functions $F^1(\lambda_i, y, z)$ and $\mathbf{G}^1(\lambda_i, y, z)$ can be generated from equations (3a) to (3c). In terms of a 'polar' coordinate introduced in the previous work [7], the governing integral equation for $F(\lambda_i, y, z)$, the volumetric radiosity or the black body emissive power, is

$$4F(\lambda_i,\eta,\zeta) = \iint_{(r,\phi)} F\left(\lambda_i,\eta+\frac{r}{L_1}\cos\phi,\zeta+\frac{r}{L_2}\sin\phi\right)S_1(r)\,dr\,d\phi + \int_{\phi_1}^{\phi_2} S_2(L_2\zeta\sec\phi)\,d\phi \quad (11)$$

where

$$\eta = \frac{y}{Y}, \quad \zeta = \frac{z}{Z}$$

$$L_1 = K_i Y, \quad L_2 = K_i Z \quad (12)$$

and

$$\phi_1 = \tan^{-1}\frac{L_1(\lambda_{i-1/2}-\eta)}{L_2\zeta} \quad (13)$$

$$\phi_2 = \tan^{-1}\frac{L_1(\lambda_{i-1/2}-\eta)}{L_2\zeta} \quad (14)$$

K_i is the extinction coefficient of the medium. The heat flux expressions are

$$G_\eta(\lambda_i,\eta,\zeta) = -\iint_{(r,\phi)} F\left(\lambda_i,\eta+\frac{r}{L_1}\cos\phi,\zeta+\frac{r}{L_2}\sin\phi\right)S_2(r)\cos\phi\,dr\,d\phi - \int_{\phi_1}^{\phi_2} S_2(L_2\zeta\sec\phi)\sin\phi\,d\phi \quad (15)$$

$$G_{\zeta}(\lambda_i,\eta,\zeta) = -\int\int_{(r,\phi)} F\left(\lambda_i,\eta+\frac{r}{L_1}\cos\phi,\zeta+\frac{r}{L_2}\sin\phi\right)S_2(r)\sin\phi\,dr\,d\phi + \int_{\phi_1}^{\phi_2} S_3(L_2\zeta\sec\phi)\cos\phi\,d\phi. \quad (16)$$

The region of integration (r, ϕ) for the above double integrations at a given (η, ζ) is illustrated by Fig. 2.

Unlike the previous work [8], the fundamental solutions will not be generated by a point allocation method in which a single polynomial is used to represent the radiosity over the whole enclosure. For improved computational efficiency and accuracy, the rectangular enclosure is broken into a finite $N+1\times N+1$ grid with the nodal temperature $F_{m,n} = F(\lambda_i, \eta_m, \zeta_n)$ where $\eta_m = m\Delta\eta$, $\zeta_n = n\Delta\zeta$, with $m, n = 0, N$ and $\Delta\eta = \Delta\zeta = 1/N$. Within each rectangular element bounded by the four points (η_m, ζ_n), (η_m, ζ_{n+1}), (η_{m+1}, ζ_n) and $(\eta_{m+1}, \zeta_{n+1})$, the emissive power distribution is assumed to be given by the following linearized expression:

$$F(\lambda_i,\eta,\zeta) = F_{m,n} + \frac{F_{m+1,n}-F_{m,n}}{\Delta\eta}(\eta-m\Delta\eta) + \frac{F_{m,n+1}-F_{m,n}}{\Delta\zeta}(\zeta-n\Delta\zeta) + \frac{F_{m+1,n+1}+F_{m,n}-F_{m+1,n}-F_{m,n+1}}{\Delta\eta\Delta\zeta}(\eta-m\Delta\eta)(\zeta-n\Delta\zeta). \quad (17)$$

Substituting equation (17) into equation (11) and evaluating at (η_i, ζ_j), a set of $N+1\times N+1$ algebraic equations for the unknown nodal temperatures can be generated as follows:

$$4F_{i,j} = \sum_{m,n=0}^{m,n=N} A_{i,j,m,n}F_{m,n} + B_{i,j}, \quad i,j = 0,1,\ldots,N. \quad (18)$$

Detailed expressions for $A_{i,j,m,n}$ and $B_{i,j}$ are given in the Appendix. In general, these coefficients are expressions involving single integrals of the general exponential integral function $S_n(x)$ which have been studied extensively in previous works [7, 8].

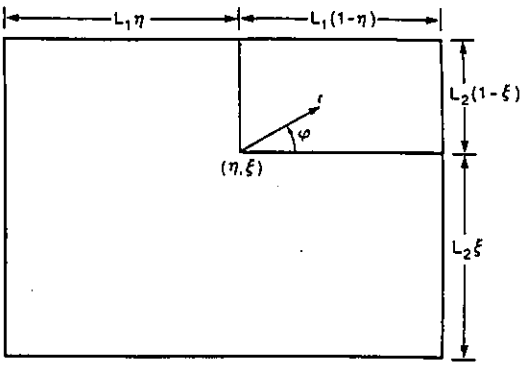

FIG. 2. Domain of integration and the 'polar' coordinate system used in equations (11), (15) and (16).

For $\Delta\lambda = 0.1$, fundamental solutions $F(\lambda_i, \eta, \zeta)$ and $G(\lambda_i, \eta, \zeta)$ are generated for $i = 0$–5 using an 11×11 grid. Fundamental solutions for $i = 6$–10 can be readily generated from the $i = 0$–5 solutions using symmetry considerations. To illustrate the quality of the numerical data, the heat flux and temperature distributions at the bottom wall for the six fundamental solutions with $L_1 = L_2 = 1.0$ are presented in Tables 1 and 2. Based on tabulated values of $S_n(x)(n = 1, 4)$, the computation is extremely efficient. Independent of optical thickness, each of the six solutions is generated with less than 1 min CPU time with a DEC VAX 11/780 computer. The accuracy of the computation is also excellent. When the six fundamental solutions are superposed to form a solution to the problem of unit normalized emissive power over the whole bottom wall, for example, the agreement with the reported

Table 1. Values of the fundamental solutions $F_i(\eta, 0)$ for an enclosure with $L_1 = L_2 = 1.0$

	η					
i	0	0.1	0.2	0.3	0.4	0.5
1	0.2576	0.0061	0.0044	0.0035	0.0028	0.0024
2	0.0136	0.5281	0.0162	0.0110	0.0085	0.0068
3	0.0097	0.0165	0.5300	0.0176	0.0120	0.0092
4	0.0077	0.0114	0.0177	0.5308	0.0182	0.0124
5	0.0063	0.0089	0.0122	0.0182	0.5312	0.0185
6	0.0052	0.0071	0.0094	0.0125	0.0185	0.5313

Table 2. Values of the fundamental solutions $G_{\zeta,i}(\eta, 0)$ for an enclosure with $L_1 = L_2 = 1.0$

	η					
i	0	0.1	0.2	0.3	0.4	0.5
1	0.4854	−0.0120	−0.0087	−0.0068	−0.0054	−0.0044
2	−0.0222	0.9461	−0.0293	−0.0198	−0.0152	−0.0120
3	−0.0156	−0.0293	0.9422	−0.0318	−0.0216	−0.0164
4	−0.0123	−0.0198	−0.0318	0.9405	−0.0330	−0.0224
5	−0.0099	−0.0151	−0.0216	−0.0330	0.9397	−0.0335
6	−0.0081	−0.0120	−0.0164	−0.0224	−0.0335	0.9395

results [2, 6, 7] generated from other techniques is to within 1%.

Compared to the point allocation technique utilized in ref. [8], the present solution technique is more efficient. Because of the presence of higher power terms ($\eta^n, \zeta^n, n > 2$) in the polynomial approximation for the emissive power, the previous calculation required extremely accurate evaluation (sometimes up to 16 significant figures) of the exponential integral function $S_n(x)$ for all values of n. The present technique, on the other hand, requires only six-figure accuracy for $S_n(x)$ with $n \leqslant 4$. The present technique can be considered an extension of the conventional zonal technique [10]; but there are two differences. First, the technique allows temperature variation within each zone. Second, energy conservation as represented by equation (11) is considered for a point in space instead of for a finite zone. These two differences and the availability of numerical values of $S_n(x)$ which were tabulated in previous works, makes the technique a 'differential zonal method'.

4. RESULTS

4.1. *Case 1: hot diffuse bottom wall and three cold diffuse walls*

Results are generated for square enclosures with different optical thicknesses ($L_1 = L_2 = 0.1, 1.0, 5.0$). The bottom wall emissivity varies as ($\varepsilon_0 = 0.1, 0.5, 1.0$). The other three walls are assumed to be either black ($\varepsilon_1 = 1.0$) or have the same emissivity as the lower wall ($\varepsilon_1 = \varepsilon_0$). Numerical data for the centerline emissive power $\theta(0.5, \zeta)$, the bottom wall heat flux $q_y(\eta, 0)$ and the right wall heat flux $q_\eta(L_1, \zeta)$ are presented in Tables 3–5.

To demonstrate the general effect of surface emissivity on temperature and heat flux distributions, isotherms and flux lines for some typical cases ($L_1 = L_2 = 1.0$, $\varepsilon_0 = 0.1, 1.0$, $\varepsilon_1 = 0.1$) are presented in Fig. 3; only half the enclosure is shown due to symmetry. As expected, temperature decreases as the emissivity of the bottom wall decreases. Large temperature slips occur at the hot–cold corner and can even be seen at the centerline, Table 3. Independent of optical thickness, temperature slip increases as the emissivity decreases. This indicates that for any optical thickness, approximations which treat radiation as a no-slip diffusion phenomenon will have significant error in predicting the heat flux and temperature distribution near the hot–cold corner. Also, the shape of the flux lines is quite insensitive to the change in emissivity. This suggests that while the net heat transfer decreases with the bottom wall emissivity, the ratio of the components of the heat flux distribution is not greatly affected.

For cases of gray walls with the same emissivity, results in Tables 3–5 show that reducing surface emissivity has the general effect of lowering the temperature and heat transfer. The temperature and heat flux distributions become more uniform and the medium is nearly isothermal. One interesting result is that the bottom wall flux curve, Table 4, does not have a maximum at the corner ($\eta = 0$) for enclosures with small optical thickness and low emissivity ($\varepsilon_0 = \varepsilon_1 = 0.1$, $L_1 = 0.1, 1.0$; $\varepsilon_0 = \varepsilon_1 = 0.5$, $L_1 = 0.1$). This is due to the low emissivity and the small lateral optical thickness. The low emissivity inhibits heat transfer to the cold side walls due to increased reflection and reduced emission. The small lateral optical thickness allows the highly reflective side walls to inhibit the heat flux over a large portion of the emitting bottom wall. Energy is forced upwards instead of

Table 3. Centerline emissive power $\theta(0.5, \zeta)$ for square enclosures ($L_1 = L_2$) of varying optical thickness, bottom wall has unit emissive power, emissivity (ε_0), other walls cold, emissivities (ε_1)

L_1	ε_0	ε_1	0	0.2	0.4	0.6	0.8	1.0
0.1	0.1	0.1	0.2719	0.2615	0.2529	0.2467	0.2429	0.2418
	0.1	1.0	0.0533	0.0397	0.0295	0.0225	0.0177	0.0141
	0.5	0.5	0.3707	0.3129	0.2674	0.2356	0.2152	0.2047
	0.5	1.0	0.2630	0.1961	0.1457	0.1111	0.0873	0.0696
	1.0	1.0	0.5179	0.3864	0.2873	0.2192	0.1722	0.1373
1.0	0.1	0.1	0.2861	0.2664	0.2514	0.2398	0.2315	0.2263
	0.1	1.0	0.0794	0.0539	0.0371	0.0256	0.0175	0.0106
	0.5	0.5	0.4454	0.3471	0.2770	0.2258	0.1890	0.1617
	0.5	1.0	0.3562	0.2430	0.1678	0.1161	0.0792	0.0480
	1.0	1.0	0.6298	0.4329	0.3000	0.2080	0.1420	0.0860
5.0	0.1	0.1	0.3490	0.2921	0.2501	0.2171	0.1919	0.1736
	0.1	1.0	0.1760	0.1069	0.0648	0.0378	0.0200	0.0061
	0.5	0.5	0.6401	0.4386	0.3009	0.2030	0.1355	0.0794
	0.5	1.0	0.5906	0.3660	0.2237	0.1312	0.0696	0.0211
	1.0	1.0	0.8280	0.5233	0.3227	0.1899	0.1009	0.0306

Table 4. Bottom wall heat flux $q_z(\eta, 0)$ for square enclosures ($L_1 = L_2$) of varying optical thickness, bottom wall has unit emissive power, emissivity (ε_0), other walls cold, emissivities (ε_1)

			η					
L_1	ε_0	ε_1	0	0.1	0.2	0.3	0.4	0.5
0.1	0.1	0.1	0.0760	0.0765	0.0767	0.0767	0.0768	0.0768
	0.1	1.0	0.0998	0.0998	0.0997	0.0997	0.0997	0.0997
	0.5	0.5	0.4138	0.4192	0.4210	0.4218	0.4222	0.4222
	0.5	1.0	0.4958	0.4940	0.4930	0.4925	0.4921	0.4920
	1.0	1.0	0.9834	0.9762	0.9725	0.9703	0.9690	0.9686
1.0	0.1	0.1	0.0751	0.0755	0.0755	0.0755	0.0755	0.0755
	0.1	1.0	0.0987	0.0979	0.0975	0.0972	0.0971	0.0970
	0.5	0.5	0.3869	0.3840	0.3806	0.3782	0.3768	0.3763
	0.5	1.0	0.4712	0.4522	0.4428	0.4373	0.4342	0.4333
	1.0	1.0	0.8958	0.8275	0.7948	0.7758	0.7655	0.7622
5.0	0.1	0.1	0.0726	0.0711	0.0700	0.0694	0.0690	0.0689
	0.1	1.0	0.0968	0.0921	0.0896	0.0882	0.0874	0.0871
	0.5	0.5	0.3456	0.2993	0.2735	0.2588	0.2507	0.2482
	0.5	1.0	0.4415	0.3563	0.3178	0.2964	0.2849	0.2813
	1.0	1.0	0.8190	0.5660	0.4660	0.4142	0.3876	0.3793

Table 5. Right wall heat flux $q_\eta(1.0, \zeta)$ for square enclosures ($L_1 = L_2$) of varying optical thickness, bottom wall has unit emissive power, emissivity (ε_0), other walls cold, emissivities (ε_1)

			ζ					
L_1	ε_0	ε_1	0	0.2	0.4	0.6	0.8	1.0
0.1	0.1	0.1	0.0275	0.0263	0.0255	0.0249	0.0244	0.0235
	0.1	1.0	0.0529	0.0419	0.0324	0.0248	0.0189	0.0143
	0.5	0.5	0.1875	0.1610	0.1401	0.1234	0.1103	0.0959
	0.5	1.0	0.2629	0.2074	0.1604	0.1226	0.0933	0.0705
	1.0	1.0	0.5213	0.4091	0.3162	0.2417	0.1840	0.1390
1.0	0.1	0.1	0.0287	0.0267	0.0252	0.0241	0.0231	0.0214
	0.1	1.0	0.0728	0.0530	0.0380	0.0268	0.0183	0.0110
	0.5	0.5	0.2216	0.1733	0.1403	0.1148	0.0948	0.0724
	0.5	1.0	0.3421	0.2408	0.1720	0.1213	0.0828	0.0497
	1.0	1.0	0.6399	0.4328	0.3079	0.2170	0.1483	0.0891
5.0	0.1	0.1	0.0314	0.0273	0.0235	0.0204	0.0178	0.0140
	0.1	1.0	0.1074	0.0653	0.0388	0.0226	0.0120	0.0039
	0.5	0.5	0.2682	0.1706	0.1144	0.0766	0.0498	0.0248
	0.5	1.0	0.4372	0.2324	0.1357	0.0786	0.0417	0.0137
	1.0	1.0	0.7412	0.3452	0.1984	0.1143	0.0606	0.0199

sideways; therefore the heat flux closer to the center of the hot wall is greater.

To further illustrate the general effect of surface emissivity on radiative heat transfer, results for the average heat flux at the bottom wall, $q_{z,b,avg}$, and the fractional heat transfer to the top wall, F_t, for a square enclosure ($L_1 = L_2$) with identical emissivity at all walls ($\varepsilon_0 = \varepsilon_1$) are shown in Figs. 4 and 5. Mathematically, $q_{z,b,avg}$ and F_t are defined as

$$q_{z,b,avg} = \int_0^1 q_z(\eta, 0)\, d\eta \tag{19}$$

$$F_t = \frac{q_{z,t,avg}}{q_{z,b,avg}} \tag{20}$$

with

$$q_{z,t,avg} = \int_0^1 q_z(\eta, L_2)\, d\eta. \tag{21}$$

Figure 4 shows that the effect of decreasing emissivity on the average bottom wall heat flux is similar to that of increasing optical thickness. Multiple reflections increase the effective path length and lead to a reduction in the average heat flux. This effect is more significant for systems with small optical thicknesses. From Fig. 5, the fractional heat transfer decreases with increasing optical thickness due to the insulating effect of the medium. For $L_1 > 0.5$ the fractional heat transfer decreases with increasing ε_0. For $L_1 < 0.5$ the

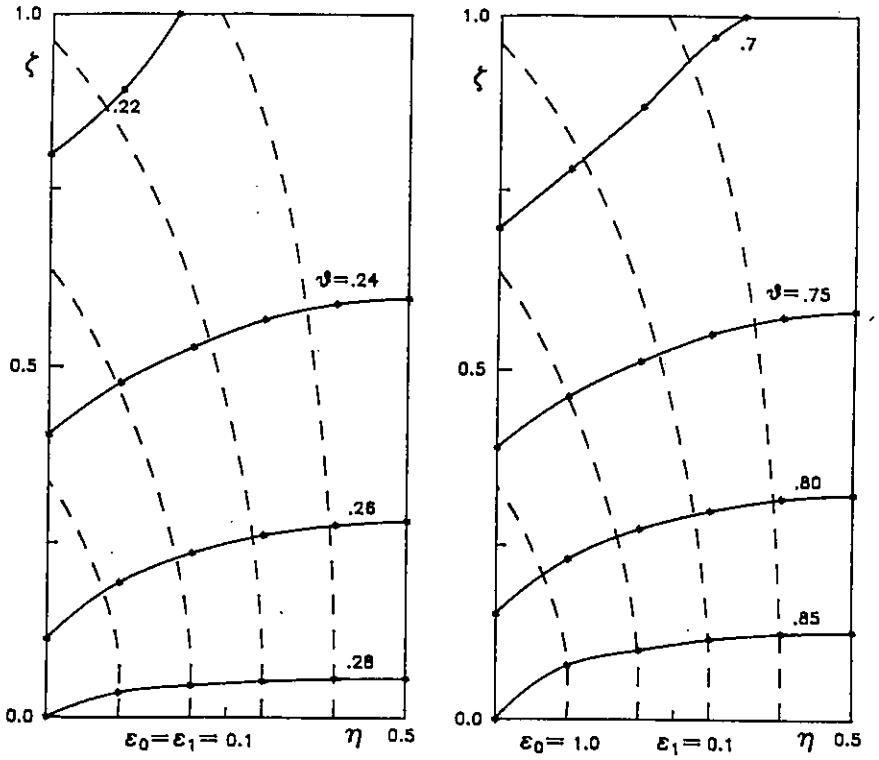

FIG. 3. $\varepsilon_0 = \varepsilon_1 = 0.1$; $\varepsilon_0 = 1.0$, $\varepsilon_1 = 0.1$. Isotherms (-*-) and flux lines (- - -) for $L_1 = L_2 = 1.0$.

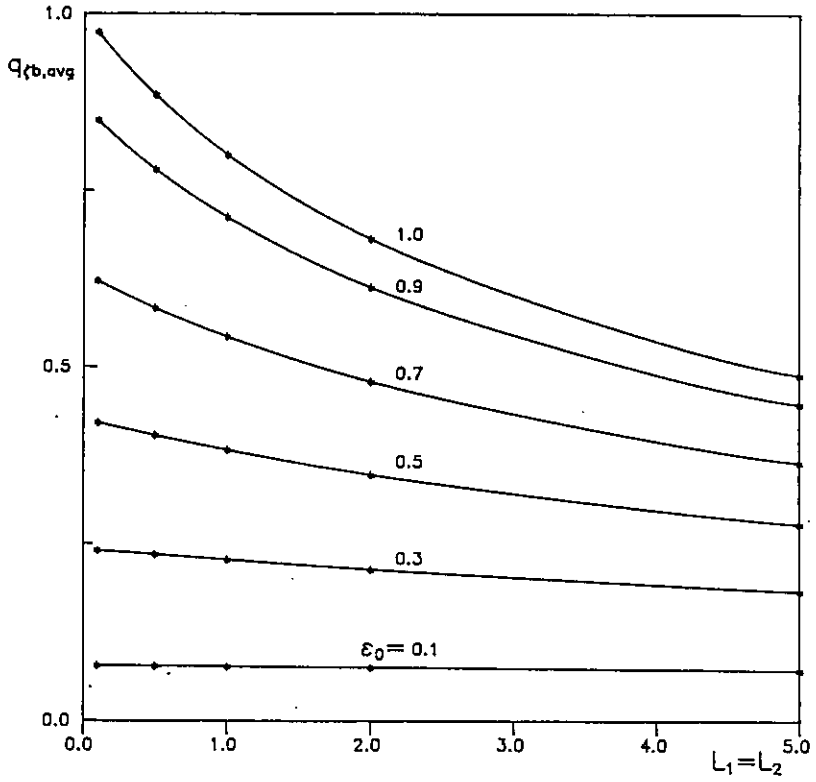

FIG. 4. Averaged bottom wall heat flux, $q_{\zeta b,avg}$, vs optical thickness, $L_1 = L_2$, $\varepsilon_0 = \varepsilon_1$ varying.

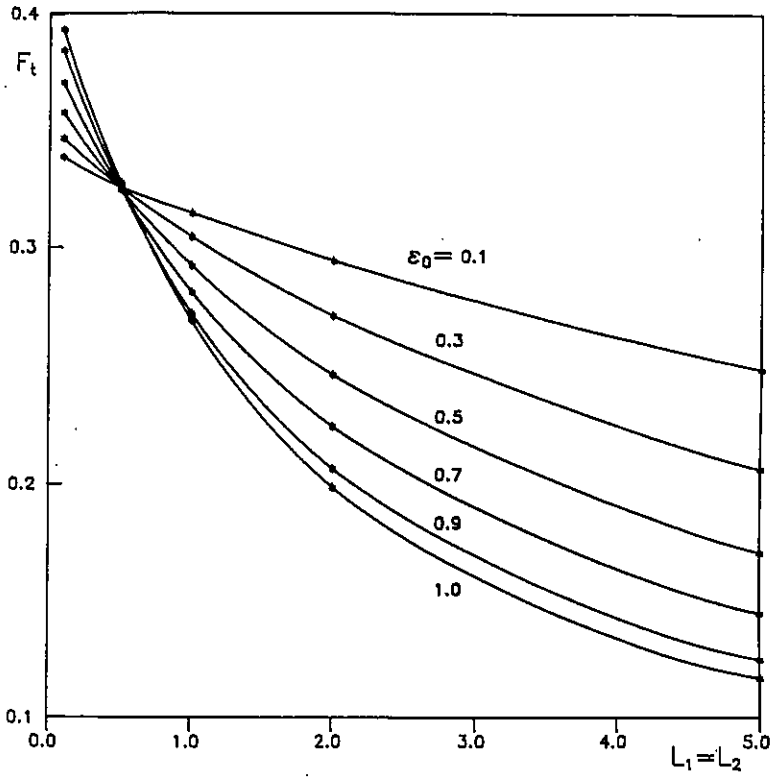

FIG. 5. Fractional heat transfer, F_t, vs optical thickness, $L_1 = L_2$, $\varepsilon_0 = \varepsilon_1$ varying.

fractional heat transfer increases with increasing ε_0. This inversion occurs because increasing the emissivity increases the amount of energy available to be absorbed by the side and top walls while the small optical thickness allows more energy to be transferred directly to the top wall, without intermediate absorption.

4.2. *Case 2: unit heat flux at bottom wall and three cold black walls*

Solutions are generated from equation (9). For square enclosures with black walls ($L_1 = L_2 = 0.1$, 1.0, 5.0), numerical data for temperature and heat flux distributions are presented in Tables 6–8. In Fig. 6 the centerline temperature distributions are presented. It should be restated that the heat flux and temperature distributions in the medium are independent of the emissivity and temperature of the bottom wall. Therefore, significant temperature slip can occur even in the optically thick limit for this class of problem. The effect of the change in optical thickness on the temperature depends on position. For points near the cold (top) wall, temperature decreases with increasing optical thickness. For points away from the cold wall temperature increases with increasing optical thickness. The fall in temperature for points near the cold wall can be attributed to increasing intermediate absorption as the optical thickness increases.

Table 6. Emissive power distribution $\theta(\eta, \zeta)$ for square enclosures with a bottom wall that is black and has unit normal heat flux, other walls black and cold

		η					
L_1	ζ	0	0.1	0.2	0.3	0.4	0.5
0.1	1.0	0.1169	0.1252	0.1320	0.1370	0.1402	0.1412
	0.5	0.1771	0.2044	0.2269	0.2436	0.2538	0.2572
	0.0	0.2656	0.5269	0.5307	0.5329	0.5342	0.5346
1.0	1.0	0.0737	0.0866	0.0960	0.1029	0.1070	0.1084
	0.5	0.1779	0.2298	0.2675	0.2946	0.3109	0.3164
	0.0	0.3622	0.7281	0.7718	0.7982	0.8128	0.8176
5.0	1.0	0.0219	0.0381	0.0507	0.0602	0.0662	0.0682
	0.5	0.1530	0.3034	0.4137	0.4946	0.5440	0.5607
	0.0	0.5422	1.4072	1.6936	1.8687	1.9669	1.9988

4.3. *Case 3: hot diffuse bottom wall, two cold diffuse walls and an adiabatic side wall*

Results generated for this case illustrate an interesting and important fundamental difference between radiative and conductive heat transfer. In conduction an adiabatic surface is a line of symmetry; this is

Table 7. Heat flux distributions $q_\eta(\eta, \zeta)$ for square enclosures with a bottom wall that is black and has unit normal heat flux, other walls black and cold

		η					
L_1	ζ	0	0.1	0.2	0.3	0.4	0.5
	1.0	−0.1430	−0.1230	−0.0976	−0.0677	−0.0347	0.0000
0.1	0.5	−0.2847	−0.2542	−0.2043	−0.1415	−0.0721	0.0000
	0.0	−0.5304	−0.0186	−0.0138	−0.0093	−0.0047	0.0000
	1.0	−0.1126	−0.0981	−0.0783	−0.0545	−0.0280	0.0000
1.0	0.5	−0.3280	−0.2890	−0.2306	−0.1592	−0.0810	0.0000
	0.0	−0.7396	−0.1487	−0.1091	−0.0720	−0.0358	0.0000
	1.0	−0.0442	−0.0421	−0.0349	−0.0248	−0.0129	0.0000
5.0	0.5	−0.3337	−0.3027	−0.2431	−0.1687	−0.0861	0.0000
	0.0	−1.1526	−0.4055	−0.2762	−0.1743	−0.0846	0.0000

Table 8. Heat flux distributions $q_\zeta(\eta, \zeta)$ for square enclosures with a lower wall that is black and has unit normal heat flux, other walls black and cold

		η					
L_1	ζ	0	0.1	0.2	0.3	0.4	0.5
	1.0	0.3314	0.3633	0.3899	0.4101	0.4228	0.4270
0.1	0.5	0.4306	0.5178	0.5919	0.6460	0.6782	0.6887
	0.0	1.0000	1.0000	1.0000	1.0000	1.0000	1.0000
	1.0	0.2000	0.2388	0.2679	0.2893	0.3026	0.3070
1.0	0.5	0.3207	0.4047	0.4762	0.5285	0.5597	0.5700
	0.0	1.0000	1.0000	1.0000	1.0000	1.0000	1.0000
	1.0	0.0516	0.0923	0.1238	0.1475	0.1622	0.1672
5.0	0.5	0.1343	0.2234	0.2986	0.3536	0.3866	0.3975
	0.0	1.0000	1.0000	1.0000	1.0000	1.0000	1.0000

not always the case in radiative heat transfer. To be considered a line of symmetry in radiative heat transfer, a surface must be both adiabatic and specular. The left-hand-side solution for an enclosure with $L_1 = 2.0$, $L_2 = 1.0$ and case 1 boundary conditions can thus be interpreted as the solution to a square enclosure $L_1 = L_2 = 1.0$ with a hot diffuse bottom wall, cold diffuse upper and left walls and a perfectly specular, adiabatic right wall. This solution is different from that with a diffuse adiabatic right wall. To illustrate the difference, isotherms and flux lines for the diffuse and specular adiabatic right walls are shown side by side in Fig. 7. Clearly the diffuse-adiabatic right wall enclosure does not have maximum temperatures at the right wall, unlike the specular/symmetric right wall enclosure. The flux lines are also much more curved for the specular/symmetric case. This indicates a larger portion of the total energy is transferred to the left side wall in the specular/symmetric case. Lastly, the temperature distribution is much sharper for the diffuse-adiabatic wall; for the diffuse-adiabatic case regions near the bottom wall are hotter and regions far away are cooler. These results show that non-diffuse behavior by the walls has a significant effect on heat flux and temperature distributions.

5. CONCLUSIONS

Based on a superposition procedure, solutions to problems of two-dimensional radiative equilibrium in a rectangular enclosure with complex boundary conditions are generated. The general effects of surface emissivity, a heat flux boundary condition, and an adiabatic specular/diffuse surface are illustrated with numerical data.

For an enclosure with specified wall temperature (a hot lower wall and three isothermal cold walls), the general conclusions are given below.

(1) The medium temperature and heat transfer decreases with decreasing emissivity at the bottom wall. Significant temperature slips occur at the hot–cold corner of the enclosure, independent of optical thickness and increasing as emissivity decreases. The medium temperature distribution is more uniform in enclosures with low surface emissivity.

(2) For an enclosure with equal surface emissivity, the heat transfer (as illustrated by F_t, the fractional heat transfer from the bottom surface to the top surface) is a sensitive function of both optical thickness and surface emissivity. F_t decreases with decreasing surface emissivity in the optically thin limit while it increases with decreasing surface emissivity in the optically thick limit.

For an enclosure with a uniform heat flux at the bottom wall, the medium temperature is shown to be independent of both the surface temperature and surface emissivity of the bottom wall. Specification of the heat flux and surface emissivity are required to determine the surface temperature in a pure radiation problem. Significant temperature slip is observed for all optical thicknesses.

For an enclosure with an insulated boundary, it was shown that the insulated boundary is not a plane of symmetry unless it is also a specular surface. Sig-

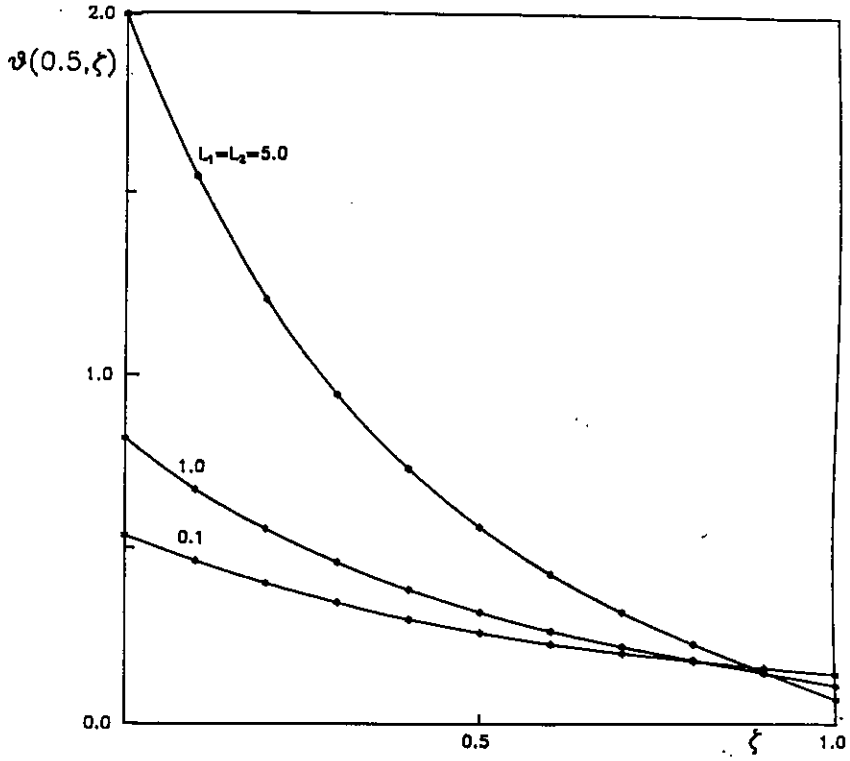

FIG. 6. Centerline temperatures for radiative heat transfer in an enclosure with unit normalized heat flux at the lower wall.

nificant difference is observed in both temperature distribution and heat transfer between results generated with an adiabatic specular boundary and those generated with an adiabatic diffuse boundary.

The results presented are a small portion of the many permutations of geometry, optical thickness and surface boundary conditions that can be handled with the method presented. For instance it is possible to handle mixed boundary condition problems where the emissivity, temperature or heat flux of a wall can be a function of position. Many two-dimensional rectangular enclosures can be analyzed with minimal

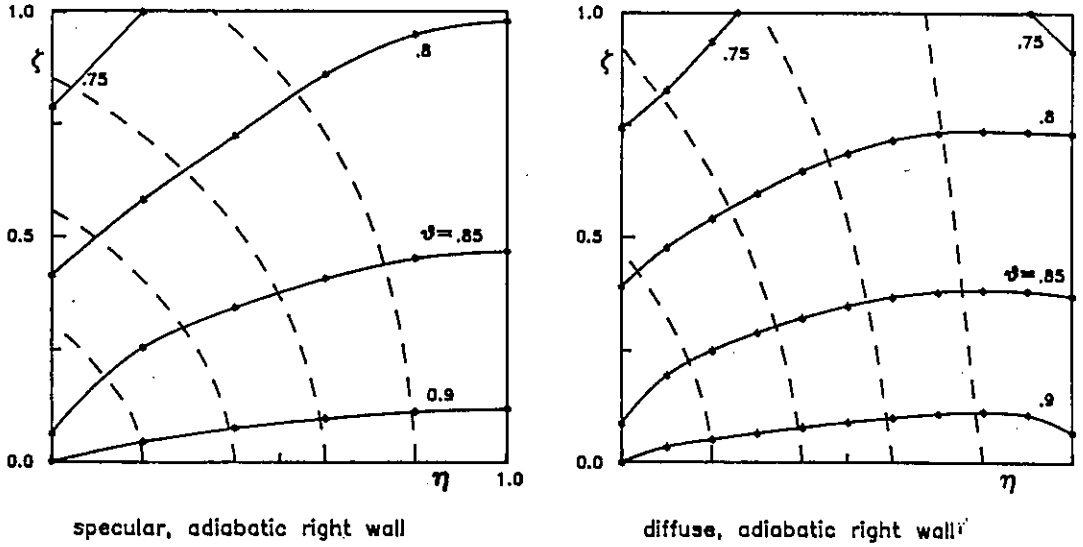

FIG. 7. Specular, adiabatic right wall; diffuse, adiabatic right wall. Isotherms (-*-) and flux lines (- - -) for $L_1 = L_2 = 1.0$, $\varepsilon_0 = 1.0$, $\varepsilon_1 = 0.1$.

effort once the fundamental solutions are generated and stored. The storage requirements using (11×11) grids for seven different enclosures are well under 1 megabyte. This method can also be extended to analyze three-dimensional enclosures.

REFERENCES

1. L. Glatt and D. B. Olfe, Radiative equilibrium of a gray medium in a rectangular enclosure, *J. Quant. Spectrosc. Radiat. Transfer* **13**, 881–895 (1973).
2. M. F. Modest, Radiative equilibrium in a rectangular enclosure bounded by gray walls, *J. Quant. Spectrosc. Radiat. Transfer* **15**, 445–461 (1975).
3. A. C. Ratzel and J. R. Howell, Two-dimensional radiation in absorbing–emitting–scattering media using the *P–N* differential approximation, ASME Paper 82-HT-19 (1982).
4. M. M. Razzaque, D. E. Klein and J. R. Howell, Finite element solution of radiative heat transfer in a two-dimensional rectangular enclosure with gray participating media, ASME Paper 82-WA/HT-61 (1982).
5. W. H. Sutton, Radiative transfer in one- and two-dimensional participating media with rectangular coordinates, Ph.D. Dissertation, North Carolina State University (1981).
6. A. L. Crosbie and R. G. Schrenker, Radiative transfer in a two-dimensional rectangular medium exposed to diffuse radiation, *J. Quant. Spectrosc. Radiat. Transfer* **31**(4), 339–372 (1984).
7. W. W. Yuen and L. W. Wong, Analysis of radiative equilibrium in a rectangular enclosure with gray medium, *ASME J. Heat Transfer* **106**(2), 433–440 (1984).
8. W. W. Yuen and C. F. Ho, Analysis of two-dimensional radiative heat transfer in a gray medium with internal heat generation, *Int. J. Heat Mass Transfer* **28**, 17–23 (1985).
9. S. T. Thynell and M. N. Ozisik, *J. Thermophys.* **1**(1), 69–76 (1987).
10. H. C. Hottel and A. F. Sarofim, *Radiative Transfer*. McGraw-Hill, New York (1967).
11. M. F. Modest, Two-dimensional radiative equilibrium of a gray medium in a plane layer bounded by gray nonisothermal walls, *ASME J. Heat Transfer* **96**, 483–488 (1974).
12. A. L. Crosbie and J. W. Koewing, Two-dimensional radiative heat transfer in a planar layer bounded by nonisothermal walls, *AIAA J.* **17**(1) 196–203 (1979).
13. J. J. Noble, The zone method: explicit matrix relations for total exchange areas, *Int. J. Heat Mass Transfer* **18**, 261–269 (1975).
14. M. E. Larsen and J. R. Howell, The exchange factor method: an alternative basis for zonal analysis of radiating enclosures, *ASME J. Heat Transfer* **107**, 936–942 (1985).
15. M. M. Razzaque, J. R. Howell and D. E. Klein, Coupled radiative and conductive heat transfer in a two-dimensional rectangular enclosure with gray participating media using finite elements, *ASME J. Heat Transfer* **106**, 613–619 (1984).
16. A. C. Ratzel and J. R. Howell, Two-dimensional energy transfer in radiatively participating media with conduction by the *P–N* approximation, *Proc. Seventh Int. Heat Transfer Conf.*, Vol. R14, pp. 535–540 (1982).
17. W. W. Yuen and E. E. Takara, Analysis of combined conductive–radiative heat transfer in a two-dimensional rectangular enclosure with a gray medium, *ASME J. Heat Transfer* **110**(2), 468–474 (1988).
18. C. N. Sokmen and M. M. Razzaque, Finite element analysis of conduction–radiation heat transfer in an absorbing–emitting and scattering medium contained in an enclosure with heat flux boundary conditions. In *Radiation Phase Change Heat Transfer, and Thermal Systems, HTD* (Edited by Y. Jaluria), Vol. 81, pp. 17–23 (1987).
19. B. Gebhart, Surface temperature calculations in radiant surroundings of arbitrary complexity— for gray, diffuse radiation, *Int. J. Heat Mass Transfer* **3**, 341–346 (1961).
20. R. Siegel and J. R. Howell, *Thermal Radiation Heat Transfer*. McGraw-Hill, New York (1972).

APPENDIX: EVALUATION OF $A_{i,j,m,n}$ AND $B_{i,j}$

At $\eta = 0$ and $\zeta = 0$, evaluation of the integrals in equation (11) over a rectangular $N+1 \times N+1$ grid can be written as sums of integrals over each of the rectangular elements. Specifically, let

$$N_{m,n}(L_1, L_2, \Delta\eta, \Delta\zeta) = \int\int_{(m,n)} F\left(\lambda_i, \frac{r}{L_1}\cos\phi, \frac{r}{L_2}\sin\phi\right) S_1(r)\, dr\, d\phi \quad \text{(A1)}$$

be an integral over a rectangular element bounded by the four points (η_m, ζ_n), (η_m, ζ_{n+1}), (η_{m+1}, ζ_n) and $(\eta_{m+1}, \zeta_{n+1})$. Utilizing equation (17), it can be readily shown that evaluation of $N_{m,n}$ requires the following four integrals:

$$H_{0,0} = \int\int_{(m,n)} S_1(r)\, dr\, d\phi \quad \text{(A2)}$$

$$H_{1,0} = \int\int_{(m,n)} S_1(r) r\cos\phi\, dr\, d\phi \quad \text{(A3)}$$

$$H_{0,1} = \int\int_{(m,n)} S_1(r) r\sin\phi\, dr\, d\phi \quad \text{(A4)}$$

$$H_{1,1} = \int\int_{(m,n)} S_1(r) r^2\cos\phi\sin\phi\, dr\, d\phi. \quad \text{(A5)}$$

Utilizing the recursive relation for $S_1(r)$, the above four integrals can be simplified into a single integral in ϕ. $H_{0,0}$, for example, becomes

$$H_{0,0} = \int_{\beta_1}^{\beta_4} S_2\left(\frac{L_2 n\Delta\zeta}{\sin\phi}\right) d\phi - \int_{\beta_2}^{\beta_4} S_2\left(\frac{L_2(n+1)\Delta\zeta}{\sin\phi}\right) d\phi + \int_{\beta_1}^{\beta_4} S_2\left(\frac{L_1 m\Delta\eta}{\cos\phi}\right) d\phi - \int_{\beta_1}^{\beta_3} S_2\left(\frac{L_1(m+1)\Delta\eta}{\cos\phi}\right) d\phi \quad \text{(A6)}$$

where

$$\beta_1 = \tan^{-1}\frac{L_2 n\Delta\zeta}{L_1(m+1)\Delta\eta} \quad \text{(A7)}$$

$$\beta_2 = \tan^{-1}\frac{L_2(n+1)\Delta\zeta}{L_1(m+1)\Delta\eta} \quad \text{(A8)}$$

$$\beta_3 = \tan^{-1}\frac{L_2 n\Delta\zeta}{L_1 m\Delta\eta} \quad \text{(A9)}$$

$$\beta_4 = \tan^{-1}\frac{L_2(n+1)\Delta\zeta}{L_1 m\Delta\eta}. \quad \text{(A10)}$$

All integrals required in the evaluation of equation (A6) and analogous expressions for $H_{0,1}$, $H_{1,0}$ and $H_{1,1}$ are of the form

$$G_{i,j,k}(x, y) = x^k \int_0^{\tan^{-1}(y/x)} S_{2+i+j-k}(x\sec\phi)\tan^i\phi\cos^{i+j-k}\phi\, d\phi. \quad \text{(A11)}$$

Previous works [7, 8] utilizing the properties of $S_n(x)$, evaluated the above integrals with little effort. In terms of the function $G_{i,j,k}(x, y)$, $H_{i,j}(i, j = 0, 1)$ can be written as

$$H_{i,j} = M_{i,j}[L_1(m+1)\Delta\eta, L_2 n\Delta\zeta] - M_{i,j}[L_1 m\Delta\eta, L_2 n\Delta\zeta] - M_{i,j}[L_1(m+1)\Delta\eta, L_2(n+1)\Delta\zeta] + M_{i,j}[L_1 m\Delta\eta, L_2(n+1)\Delta\zeta] \quad (A12)$$

with

$$M_{i,j}(x, y) = \sum_{k=0}^{i+j} \frac{(i+j)!}{k!}(G_{i,j,k}(x, y) + G_{i,j,k}(y, x)). \quad (A13a)$$

Since $G_{i,j,k}(0, 0)$ is undefined, $M_{i,j}(0, 0)$, which is required in the evaluation of equation (A12) when $m = n = 0$, is interpreted as

$$M_{i,j}(0, 0) = \lim_{\sigma \to 0} M_{i,j}(0, \sigma). \quad (A13b)$$

Using equation (17), $N_{m,n}(L_1, L_2, \Delta\eta, \Delta\zeta)$ can be written as

$$N_{m,n}(L_1, L_2, \Delta\eta, \Delta\zeta) = P^{0,0}_{m,n}F_{m,n} + P^{0,1}_{m,n}F_{m,n+1} + P^{1,0}_{m,n}F_{m+1,n} + P^{1,1}_{m,n}F_{m+1,n+1} \quad (A14)$$

where

$$P^{0,0}_{m,n} = (1+m+n+mn)H_{0,0} - (1+n)\frac{H_{1,0}}{L_1\Delta\eta} - (1+m)\frac{H_{0,1}}{L_2\Delta\zeta} + \frac{H_{1,1}}{L_1L_2\Delta\eta\Delta\zeta} \quad (A15)$$

$$P^{1,0}_{m,n} = -(m+mn)H_{0,0} + (1+n)\frac{H_{1,0}}{L_1\Delta\eta} + \frac{mH_{0,1}}{L_2\Delta\zeta} - \frac{H_{1,1}}{L_1L_2\Delta\eta\Delta\zeta} \quad (A16)$$

$$P^{0,1}_{m,n} = -(n+mn)H_{0,0} + (1+m)\frac{H_{0,1}}{L_2\Delta\zeta} + \frac{nH_{1,0}}{L_1\Delta\eta} - \frac{H_{1,1}}{L_1L_2\Delta\eta\Delta\zeta} \quad (A17)$$

$$P^{1,1}_{m,n} = mnH_{0,0} - \frac{nH_{1,0}}{\Delta\eta L_1} - \frac{mH_{0,1}}{\Delta\zeta L_2} + \frac{H_{1,1}}{L_1L_2\Delta\eta\Delta\zeta}. \quad (A18)$$

By a simple coordinate transformation, the above results can also be applied to the evaluation of an integral over a rectangular element with respect to an arbitrary point (η_j, ζ_j).

The coefficients $A_{i,j,m,n}$ can now be evaluated in terms of $P^{i,j}_{m,n}$. The specific relations are

$$A_{i,j,m,n} = 4P^{0,0}_{0,0}, \quad m = i, n = j \quad (A19a)$$

$$A_{i,j,m,n} = 2(P^{0,0}_{0,n-j} + P^{0,1}_{0,n-j-1}), \quad m = i \quad (A19b)$$

$$A_{i,j,m,n} = 2(P^{0,0}_{m-i,0} + P^{1,0}_{m-i-1,0}), \quad n = j \quad (A19c)$$

$$A_{i,j,m,n} = P^{0,0}_{m-i,n-j} + P^{1,0}_{m-i-1,n-j} + P^{0,1}_{m-i,n-j-1} + P^{1,1}_{m-i-1,n-j-1} \quad (A19d)$$

when $ni \neq 0$, N and $n \neq 0$, N;

$$A_{i,j,m,n} = 2P^{0,0}_{0,0}, \quad m = i, n = j \quad (A20a)$$

$$A_{i,j,m,n} = 2P^{0,1}_{0,n-j-1}, \quad m = i \quad (A20b)$$

$$A_{i,j,m,n} = P^{0,0}_{m-i,0} + P^{1,0}_{m-i-1,0}, \quad n = j \quad (A20c)$$

$$A_{i,j,m,n} = P^{0,1}_{m-i,n-j-1} + P^{1,1}_{m-i-1,n-j-1} \quad (A20d)$$

when $m \neq 0$, N and $n = 0$, N;

$$A_{i,j,m,n} = 2P^{0,0}_{0,0}, \quad m = i, n = j \quad (A21a)$$

$$A_{i,j,m,n} = P^{0,0}_{0,n-j} + P^{0,1}_{0,n-j-1}, \quad m = i \quad (A21b)$$

$$A_{i,j,m,n} = 2P^{1,0}_{m-i-1,0}, \quad n = j \quad (A21c)$$

$$A_{i,j,m,n} = P^{1,0}_{m-i-1,n-j} + P^{1,1}_{m-i-1,n-j-1} \quad (A21d)$$

when $m = 0$, N and $n \neq 0$, N;

$$A_{i,j,m,n} = P^{0,0}_{0,0}, \quad m = i, n = j \quad (A22a)$$

$$A_{i,j,m,n} = P^{0,1}_{0,n-j-1}, \quad m = i \quad (A22b)$$

$$A_{i,j,m,n} = P^{1,0}_{m-i-1,0}, \quad n = j \quad (A22c)$$

$$A_{i,j,m,n} = P^{1,1}_{m-i-1,n-j-1} \quad (A22d)$$

when $m = 0$, N and $n \neq 0$, N.

The above coefficients are applicable for all fundamental solutions. $B_{i,j}$, on the other hand, varies for the different fundamental solutions. For $F(\lambda_j, \eta, \zeta)$, $B_{i,j}$ is given by

$$B_{i,j} = G_{0,0,0}(L_2 j\Delta\zeta, L_1(\lambda_{i+1/2} - i\Delta\eta)) - G_{0,0,0}(L_2 j\Delta\zeta, L_1(\lambda_{i-1/2} - i\Delta\eta)). \quad (A23)$$

After equation (18) is solved, the fundamental heat flux $G(\lambda_j, \eta, \zeta)$ can be generated from equations (15) and (16) utilizing a similar procedure for the evaluation of the required integrals.

It is important to emphasize that evaluation of the function $G_{i,j,k}(x, y)$ is the only required numerical integration in the present solution procedure. As demonstrated in previous works [7, 8], $G_{i,j,k}(x, y)$ satisfies a set of recursive relations. For the few integrals which need to be evaluated numerically, the computation generally requires little effort.

TECHNIQUE DE SUPERPOSITION POUR L'EQUILIBRE RADIATIF DANS DES CAVITES RECTANGULAIRES AVEC DES CONDITIONS AUX LIMITES COMPLEXES

Résumé—On utilise la superposition des solutions fondamentales pour trouver les distributions de flux thermique et de température dans des cavités rectangulaires bidimensionnelles à parois grises avec un milieu gris absorbant et émissif, à diffusion isotrope. Les solutions fondamentales concernent les cavités avec des frontières noires et un changement d'échelon de température sur un intervalle fini de paroi. Elles sont obtenues en utilisant une variation de la méthode conventionnelle de zonage. Des distributions fines de flux thermique et de température pour les cas typiques sont présentées pour illustrer la simplicité de la procédure de superposition. Sur la base de ces résultats, on discute les effets des conditions aux limites sur la distribution de température et de transfert de chaleur.

ÜBERLAGERUNGSMETHODE FÜR STRAHLUNGSGLEICHGEWICHTE IN RECHTECKIGEN RÄUMEN MIT KOMPLEXEN RANDBEDINGUNGEN

Zusammenfassung—Die Überlagerung von Grundgleichungen wird angewendet, um Temperatur- und Wärmestromverteilungen in rechtwinkligen zweidimensionalen Räumen mit grauen Wänden und einem grau strahlenden, isotrop streuenden Medium zu berechnen. Als Lösung ergeben sich Temperatur- und Wärmestromverteilungen für Räume mit schwarzen Wänden und in einem endlichen Wandabschnitt stufenweise veränderte Temperaturen. Dabei wird eine Variation der üblichen Zonen-Methode angewandt. Detaillierte Wärmestrom- und Temperaturverteilungen werden für grundlegende Fälle vorgestellt, um die einfache Anwendbarkeit der Überlagerungsmethode zu zeigen. Von diesen Ergebnissen ausgehend, wird der Einfluß der Randbedingungen an der Oberfläche auf die Temperatur- und Wärmestromverteilung diskutiert.